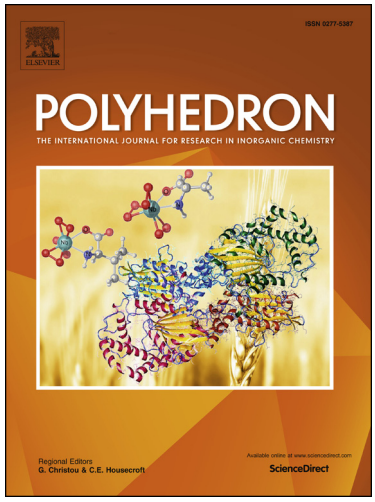

Fluorenyl-Schiff-base ligands and their dicopper(II) complexes. Synthesis, structural and spectroscopic characterization and DNA binding assays

Fabiane dos Santos Carlos, Marcelo Carpes Nunes, Bernardo Almeida Iglesias, Priscilla J. Zambiazi, Manfredo Hörner, Guilherme A. de Moraes, Guilherme Sippel Machado, Ronny Rocha Ribeiro, Fábio Souza Nunes

PII: S0277-5387(18)30003-2
DOI: https://doi.org/10.1016/j.poly.2018.01.003
Reference: POLY 12995

To appear in: *Polyhedron*

Received Date: 30 August 2017
Revised Date: 17 November 2017
Accepted Date: 2 January 2018

Please cite this article as: F.d.S. Carlos, M.C. Nunes, B.A. Iglesias, P.J. Zambiazi, M. Hörner, G.A. de Moraes, G.S. Machado, R.R. Ribeiro, F.S. Nunes, Fluorenyl-Schiff-base ligands and their dicopper(II) complexes. Synthesis, structural and spectroscopic characterization and DNA binding assays, *Polyhedron* (2018), doi: https://doi.org/10.1016/j.poly.2018.01.003

Fluorenyl-Schiff-base ligands and their dicopper(II) complexes. Synthesis, structural and spectroscopic characterization and DNA binding assays

Fabiane dos Santos Carlos,[a] Marcelo Carpes Nunes,[a] Bernardo Almeida Iglesias,[b] Priscilla J. Zambiazi,[b] Manfredo Hörner,[b] Guilherme A. de Moraes,[b] Guilherme Sippel Machado,[c] Ronny Rocha Ribeiro[a] and Fábio Souza Nunes[a]*

[a]*Departamento de Química, Universidade Federal do Paraná, Cx. Postal 19081, 81531–980 Curitiba, PR, Brazil*

[b]*Departamento de Química, Universidade Federal de Santa Maria, 97105-900, Santa Maria, RS, Brazil*

[c]*Centro de Estudos do Mar, Universidade Federal do Paraná, Pontal do Paraná, Cx. Postal 61, 83255-976, PR, Brazil*

* *Correspondence to*: Fábio S. Nunes (fsnunes@ufpr.br)

FAX 55-41-3361-3186

Abstract

Schiff-base ligands L1 and L2 containing fluorene as fluorophore were synthesized thorough condensation of salicylaldehyde and 2,6-diformyl 4-methylphenol with 6-(9-fluorenyl)-1,4,8,11-tetraazaundecane-5,7-dione, respectively. A comprehensive spectroscopic analysis was performed by elemental analysis, ESI-MS, ^{1}H- and ^{13}C-NMR, FTIR, EPR, UV-Vis and emission spectroscopies. Ligand L1 binds copper(II) to form $[Cu_2(L1)_2]\cdot 2H_2O$ that crystallizes in orthorhombic system and space group $P2_1/n$. Assignments to the UV-vis and EPR spectra allowed access to Jahn-Teller stabilization energies (E_{JT}) at 6345 and 5435 cm^{-1} for complexes $[Cu_2(L1)_2]\cdot 2H_2O$ and $[Cu_2(L2)](ClO_4)_4\cdot 4H_2O$, respectively, and to their corresponding spin orbit coupling constants λ = -428 and -398 cm^{-1}. The EPR spectrum of $[Cu_2(L2)](ClO_4)_4\cdot 4H_2O$ in the solid state showed a half-field $\Delta m_S = \pm 2$ transition, supporting the dicopper composition. The fluorenyl copper(II) derivatives demonstrated a moderate binding to ct-DNA than the fluorenyl-ligand molecule following the increasing order of (K_b): L1 < $[Cu_2(L1)_2]\cdot 2H_2O$ < $[Cu_2(L2)](ClO_4)_4\cdot 4H_2O$.

Keywords: Schiff-base ligands; Binuclear copper complex; 6-(9-Fluorenyl)-1,4,8,11-tetraazaundecane-5,7-dione, salicylaldehyde; 2,6-Diformyl 4-methylphenol

1. Introduction

Copper is an essential element, but it is also a pollutant and can be toxic when in high concentrations in the environment [1]. Copper concentration in the environment varies and comes from natural occurrence, mining and industrial activity. Literature

presents several fluorescent sensors for copper ion, with varying degrees of sensitivity, selectivity and difficulty of preparation [2-19].

Condensation of 2,6-diformyl-4-methylphenol and diamines produces Robson-type ligands that have been investigated over the years because their coordination compounds show interesting magnetic, redox and structural properties [20-25].

Continuing our general interest in the synthesis of metal complexes of polyfunctional ligands we have recently reported the structural, magnetic and spectroscopic properties of a *bis*(semicarbazone) series prepared by Schiff condensation of 2,6-diformyl 4-methylphenol with semicarbazide hydrochloride in 1:2 molar ratio [21].

In this work we report on the preparation, characterization and properties of two coordination compounds that contain luminescent ligands **(**Scheme 1). Ligands **1** and **2** were prepared by connecting a diamidodiamine (6-(9-fluorenyl)-1,4,8,11-tetraazaundecane-5,7-dione) to two equivalents of salicylaldehyde and 2,6-diformyl-4-methylphenol, respectively. Both ligands contain fluorene, which is a fluorophore with recognized photophysical properties [26-30]. Despite of its binding ability, few papers on appending fluorescent groups to the diamidodiamine unit have been reported [26, 33]. Also, DNA-binding assays were conducted to better investigate the interaction type of this biomolecule.

2. Experimental

2.1. Preparations

The chemicals used in this work were purchased from Sigma-Aldrich and used as supplied. 6-(9-fluorenil)-1,4,8,11-tetraazaundecano-5,7-dione and 2,6-diformyl-4-methyl-phenol were prepared as described elsewhere [26,34].

Ligand **L1 (**Scheme 1) and ***[Cu$_2$(L1)$_2$]·2H$_2$O*** were synthesized according to Luo *et al*. [35]. Elemental analysis calculated(found) for L1, $C_{34}H_{32}N_4O_4$, 560.64 g mol^{-1}: C% 72.85 (72.84); H% 5.66 (5.75); N% 10.26 (10.00). ^{1}H-NMR (δ in ppm): 7.835, d, H1; 7.885, t, H2; 7.196, t, H3; 7.412, d, H4; 4.662, d, H5; 2.851, d, H6; 3.497-3.676, m, H8 and H9; 8.390, s, H10; 6.868, m, H11 and H12; 7.321, m, H13, H14 and H15. ESI-MS (negative mode) at m/z: Calculated(observed) for [L1-H]$^-$: 559.63(559.53). Yield for $[Cu_2(L1)_2]\cdot 2H_2O$ was 0.071 g, 28%. Elemental analysis calculated(found) for $C_{68}H_{64}N_8O_{10}Cu_2$,1280 g mol^{-1}: C% 63.99 (63.79); H% 4.74 (4.64); N% 9.00 (8.78).

Ligand L2 was prepared by template method. $Mg(NO_3)_2\cdot 6H_2O$ (1.00 g, 3.9 mmol) and 0.69 g (1.95 mmol) 6-(9-fluorenil)-1,4,8,11-tetraazaundecano-5,7-dione were dissolved in 30 mL of methanol and mixed with a solution of 0.32 g (1.95 mmol) of 2,6-diformyl-4-methylformol in 10 mL of methanol. The system was kept under reflux for 24h, resulting in an orange solution. One third of the volume was removed under vacuum and 20 mL of diethyl ether was added. The orange product was collected by filtration, washed with ether and dried under vacuum. Yield was 0.73 g (30%). Elemental analysis calculated(found) for $C_{58}H_{56}Mg_2N_{12}O_{18}$, 1257,75 g mol^{-1}: C% 55.54 (55.48); H% 4.42 (4.33); N% 13.17 (13.39). ^{1}H-NMR (δ in ppm): 7.195-8.534, m, H1; 4.655, d, H2; 3.311-3.352, m, H4; 3.012, d, H3; 2.775-2.857, m, H5; 2.156-2.350, m, H6. ESI-MS (positive mode) at m/z: Calculated(observed) for [L2+H]$^+$: 961.44(961.44).

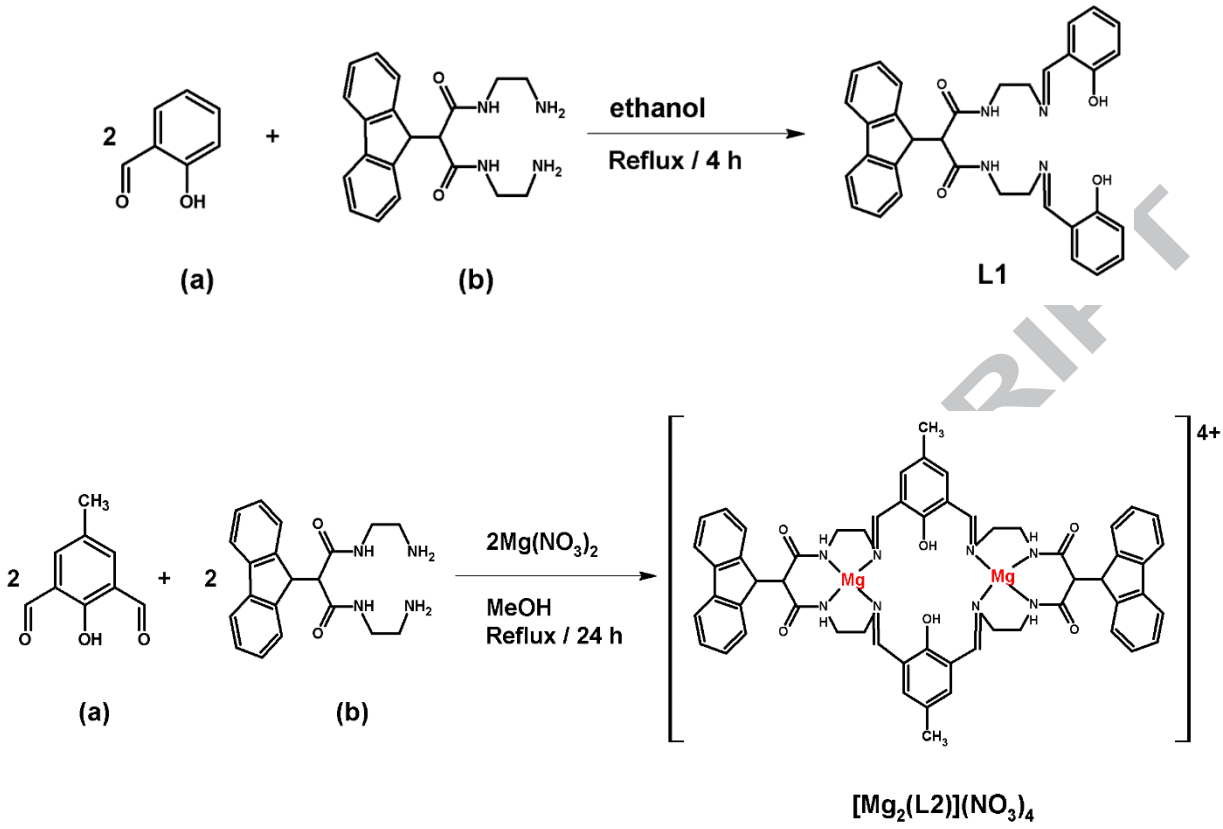

Scheme 1. Synthesis of L1 (top) and $[Mg_2(L2)](NO_3)_4$ (bottom).

[Cu$_2$(L2)(ClO$_4$)$_4$·4H$_2$O. Copper perchlorate hexahydrate (0.088 g, 0,24 mmol) dissolved in 3 mL of methanol was mixed to $[Mg_2(L2)](NO_3)_4$ (0.300 g, 0.24 mmol) in 3 mL of methanol. After reflux for 2h, the pH was set to 9 using triethylamine, and reflux was maintained for two more hours. After filtration, 2/3 of the volume was removed, leading to a brown powder, which was collected, washed with cold ethanol and dried under vacuum. Yield was 0.328 g, 88%. Elemental analysis calculated(found) for $C_{58}H_{60}N_8O_{26}Cl_4Cu_2$,1558 g mol^{-1}: C% 44.35 (44.83); H% 4.06 (4.14); N% 7.46 (7.21).

2.2. Apparatus

Elemental analyses were done in a Perkin-Elmer 2400 analyzer. Mass spectra were measured in a high resolution ESI-MS on a microTOF QII mass spectrometer (Bruker Daltonics, Billerica, MA) from dimethylsulfoxide solutions. ^{1}H and ^{13}C NMR spectra were recorded in a Bruker Avance HD spectrometer at 400 MHz, DMSO was used as solvent and TMS as the internal reference. The chemical shifts are expressed in δ (ppm).

Electronic spectra in the UV-Vis range (190-820 nm) were obtained on a diode array Hewlett-Packard 8452A or Varian Cary 50 spectrophotometer in dimethylsufoxide solutions using a 1.0 cm path length quartz cell.

Fluorescence measurements and fluorescence quantum yields were recorded in a 1.0 cm optical path length of a quartz cuvette using a Varian Cary Eclipse or Shimadzu RF5301-PC spectrofluorimeter with a concentration of $1x10^{-5}$ $mol.L^{-1}$ to minimize the re-absorption. The equipment was set at 1.5 nm slit width and 600 $nm.min^{-1}$ scan rate for both excitation and emission spectra. The solutions were always purged with nitrogen prior to the measurements to avoid quenching by dioxygen molecules. Re-absorption of the fluorescence was minimized using absorbance values smaller than 0.100 for a standard 1.0 cm optical path length quartz cuvette.

Green crystals were isolated after the slow diffusion of layers of water and methanol into a dimethylsulfoxide solution of $[Cu_2(L1)_2]$. A single crystal fixed on a glass fiber was used for the X-ray data collection. Data were collected with a Bruker APEX II CCD area–detector diffractometer and graphite–monochromatized Mo-K_α radiation using *COSMO* program [36]. Cell refinement, data reduction and the absorption correction were performed using *SAINT* and *SADABS* programs, respectively [36]. The structure of complex **1** were solved by direct methods [37] and refined on F^2

with anisotropic temperature parameters for all non H atoms [38]. The crystallographic parameters and details of data collection and refinement are given in Table 1. Further details about structure refinement can be found in the Supplementary Section.

2.3. DNA-binding experiments

Fluorenyl ligand and copper(II) compounds interactions with calf-thymus DNA (ct-DNA) were performed by spectral measurements at room temperature in phosphate buffer (PBS) at pH 7.4, using DMSO stock solution of derivatives (10^{-4} mol.L^{-1} range). The DNA pair base concentrations of low molecular weight DNA from calf thymus DNA was determined by spectroscopy, using the molar extinction coefficients 6.600 L.mol^{-1}.cm^{-1} at λ = 260 nm, respectively.

Compound solutions in dimethylsulfoxide with PBS buffer were titrated with increasing concentrations of ct-DNA (0-100 μmol.L^{-1}). The absorption spectra of derivatives were acquired in the wavelength range of 300-800 nm. The intrinsic binding constants (K_b) of fluorenyl compounds were calculated according to the decay of the absorption bands of compounds using the following Equation (1) through a plot of [DNA]/(ε_a - ε_f) *versus* [DNA]:

$$[DNA]/(\varepsilon_a - \varepsilon_f) = [DNA]/(\varepsilon_b - \varepsilon_f) + 1/K_b(\varepsilon_b - \varepsilon_f) \quad (1)$$

where [DNA] is the concentration of ct-DNA in the base pairs, ε_a is the extinction coefficient (A_{obs}/[compound]), ε_b and ε_f are the extinction coefficients of free and fully bound forms, respectively. In plots of [DNA]/(ε_a - ε_f) versus [DNA], K_b is given by the slope/interception ratio.

In the emission fluorescence analysis with ct-DNA, compounds were dissolved in DMSO and competitive studies were performed through the gradual addition of the stock solution of the derivatives to the quartz cuvette (1.0 cm path length) containing ethidium bromide (EB, 2.0 x 10^{-7} mol.L^{-1}) and DNA (1.0 x 10^{-5} mol.L^{-1}) in a PBS buffer solution. The concentration of compounds ranged from 0 to 100 μmol.L^{-1}. Samples were excited at λ_{exc} = 510 nm and emission spectra were recorded at the range of 550-800 nm, 3 min after each addition of the complex solution in order to allow incubation to occur. To distinguish the type of quenching mechanism and the extent of quenching, the Stern–Volmer type Equation (2) can be used [39]:

$$F_0/F = 1 + k_q\tau_0[Q] = 1 + K_{SV}[Q] \qquad (2)$$

where, F_0 is the original fluorescence intensity; F is the quenched intensity of the fluorophore in the presence of the compound (quencher); Q is the quencher, K_{sv} is the Stern–Volmer quenching constant; k_q is the apparent bimolecular quenching rate constant and equal to K_{sv}/τ_0.

3. Results and discussion

Structural description of $[Cu_2(L1)_2]\cdot 2H_2O$

Suitable crystals for X-ray analysis were obtained after diffusion of water and methanol into the dimethylsulfoxide solution of $[Cu_2(L1)_2]\cdot 2H_2O$. Figure 1 shows the representation of the molecular structure of the $[Cu_2(L1)_2]$ unit in $[Cu_2(L1)_2]\cdot 2H_2O$. Crystal structure analysis reveals that two units of L1 bind two copper(II) ions in a 2N2O fashion, through phenolate and imine groups. The flexible ligand is wrapped around the metal center, which is tetracoordinated and experiences a distorted square planar geometry. Main angles are O1-Cu1-N1, O1-Cu1N11, N1-Cu1-O11 and N11-Cu1-O11 at 92.9(4), 90.3(3), 91.8(4) and 94.2(4)^o, respectively. The crystallographic parameters and details of data collection and refinement are given in Table 1. Selected bond distances and angles are listed in Table 2. Li and co-workers [35] reported on the crystal structure of the monohydrate complex $[Cu_2(L1)_2]\cdot H_2O$ that crystallizes in the monoclinic system and space group $P2_1/n$. Therefore, it is different from the dihydrate compound ($[Cu_2(L1)_2]\cdot 2H_2O$) herein described, which shows an overall composition of $C_{68}H_{64}Cu_2N_8O_{10}$, a molecular mass of 1280 g.mol^{-1} and, forms orthorhombic crystals in the space group *Pccn*.

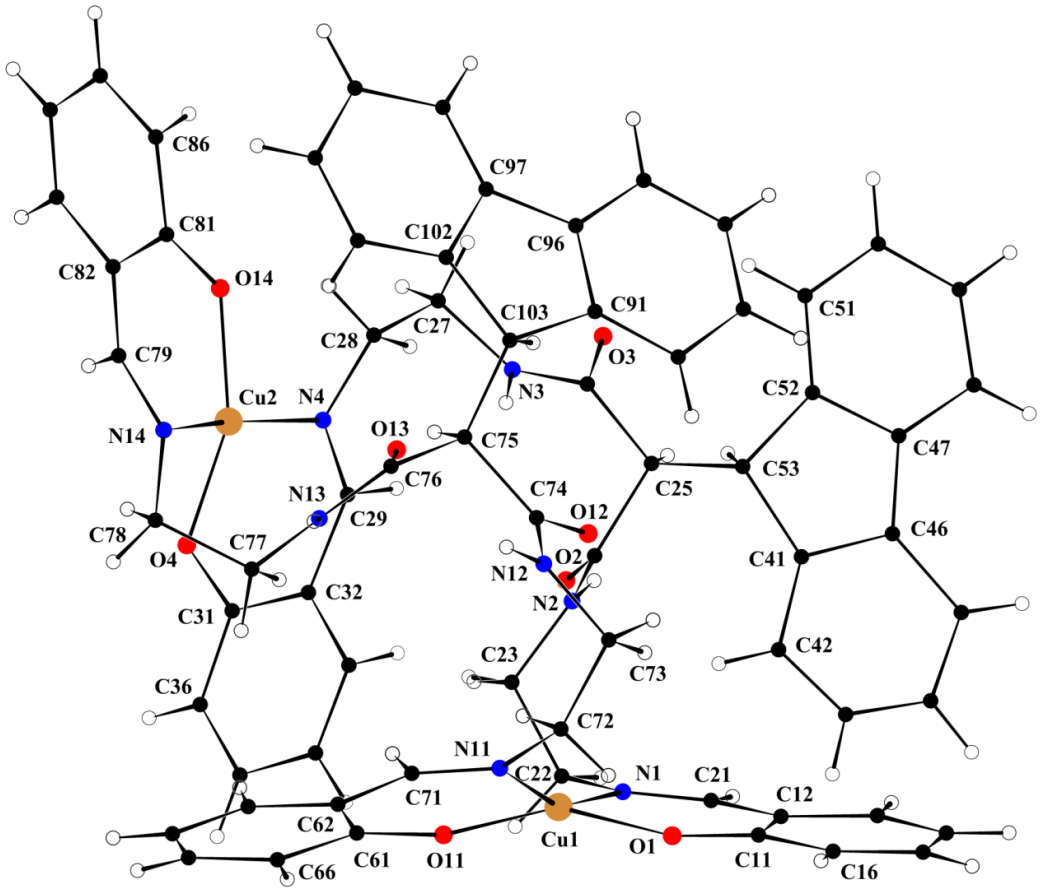

Figure 1. Projection of the molecular structure of the $[Cu_2(L1)_2]$ unit in $[Cu_2(L1)_2]\cdot 2H_2O$ with the atom labeling scheme. [40]. Atoms represented with arbitrary radii. Water molecules as crystallization solvents were omitted for clarity.

Table 1. Crystal data and structure refinement for $[Cu_2(L1)_2]\cdot 2H_2O$.

Empirical formula	$C_{68}H_{64}Cu_2N_8O_{10}$
Formula weight, g.mol^{-1}	1280.35
T (K)	296(2)
Radiation, λ / (Å)	1.54178
Crystal system, space group	Orthorombic, *Pccn*
Unit cell dimensions, *a*, *b*, *c* /Å	a = 27.6139(10)
	b = 19.5971(7)
	c = 27.5767(10)
Volume /Å^3	14923.2(9)
Z, Calculated Density /g.cm^{-3}	8, 1.140
Absorption coefficient /mm^{-1}	1.154
F(000)	5328
Crystal size (mm^3)	0.305 x 0.294 x 0.144
Theta range /°	2.765 to 60.189
Index ranges	$-30 \le h \le 30$
	$-22 \le k \le 22$
	$-31 \le l \le 30$
Reflections collected	199757
Independent reflections	11076 [R_{int} =0.0756]
Completeness to theta max	99.3%
Refinement method	Full-matrix least–squares on F^2
Data / restraints / parameters	11057 /42/781
Goodness-of-fit on F^2	1.513
Final R indices [$I > 2\sigma(I)$]	$R1$ = 0.1425,
	$wR2$ = 0.3893
R indices (all data)	$R1$ = 0.1978,
	$wR2$ = 0.4138
Largest diff. peak and hole /e.Å^{-3}	1.915 and -0.743 e.Å^{-3} *

* Highest peak 1.91 at 0.2874 0.7607 0.1616 [3.28 Å from H86].

*Deepest hole -0.74 at 0.4307 0.0990 0.0466 [0.20 Å from O15].

Table 2. Selected bond lengths / Å and angles / ° for $[Cu_2(L1)_2]\cdot 2H_2O$.

O(1)-Cu(1)	1.880(7)	O(1)-Cu(1)-N(1)	92.9(4)
O(11)-Cu(1)	1.880(8)	O(1)-Cu(1)-N(11)	90.3(3)
N(1)-Cu(1)	1.964(10)	O(11)-Cu(1)-N(1)	91.8(4)
N(11)-Cu(1)	1.963(8)	O(11)-Cu(1)-N(11)	94.2(4)
O(4)-Cu(2)	1.888(6)	O(11)-Cu(1)-O(1)	155.2(3)
O(14)-Cu(2)	1.883(7)	N(11)-Cu(1)-N(1)	158.2(3)
N(4)-Cu(2)	2.007(8)	O(14)-Cu(2)-O(4)	154.5(3)
N(14)-Cu(2)	1.968(9)	O(14)-Cu(2)-N(14)	93.5(3)

symmetry transformations used to generate equivalent atoms: (′) -1+*x*, *y*, *z*.

Despite the fact that compound $[Cu_2(L1)_2]\cdot 2H_2O$ presents two water molecules as crystallization solvates, curiously, the crystal structure of the complex shows predominantly intramolecular hydrogen bonding, while the bifurcated intermolecular hydrogen bondings discussed below, do not include the crystallization solvates. The crystal structure of $[Cu_2(L1)_2].2H_2O$ in the centrosymmetric *Pccn* space group, reveals an infinite one-dimensional 1D-chain with the base vector [010]. $[Cu_2(L1)_2]$ molecules are related by a two-fold screw axis along the [010] crystallographic direction with screw component [0,1/2,0]. The 1D chain results from hydrogen bonds with a bifurcated acceptor geometry (D_1–H_1, D_2–H_2)···*A* (*D* = donor atom, *A* = acceptor atom), (N12-H12, C75–H75)···O3′, symmetry code (′) 1-*x*, -1/2+*y*, 1/2-*z* (Figure 2). Tab. 3 lists the geometrical parameters of the bifurcated hydrogen bonding, which presents a classical hydrogen bonding component N12-H12···O3′, and, a non-classical hydrogen bonding component C75–H75···O3′, respectively connected to the same acceptor O3′ atom. Fig. 2 depicts a section of the supramolecular arrangement of the $[Cu_2(L1)_2]$ molecules in the unit cell of $[Cu_2(L1)_2]\cdot 2H_2O$ as discussed above, symmetry codes (′):1-*x*, -1/2+*y*, 1/2-*z* ; (″): *x*, -1+*y*, *z* ; (‴): 1-*x*, 1/2+y, 1/2-z).

Table 3. Hydrogen-bonding geometric parameters (Å, °)

D–H···*A*	*D*–H	H···*A*	*D*···*A*	*D*–H···*A*
N12–H12···O3′	0.86	2.080	2.914(9)	163.15
C75–H75···O3′	0.98	2.560	3.413(10)	149.49

(*D* = donor atom, *A* = acceptor atom)

Symmetry code: (′) 1-*x*, -1/2+*y*, 1/2-*z*

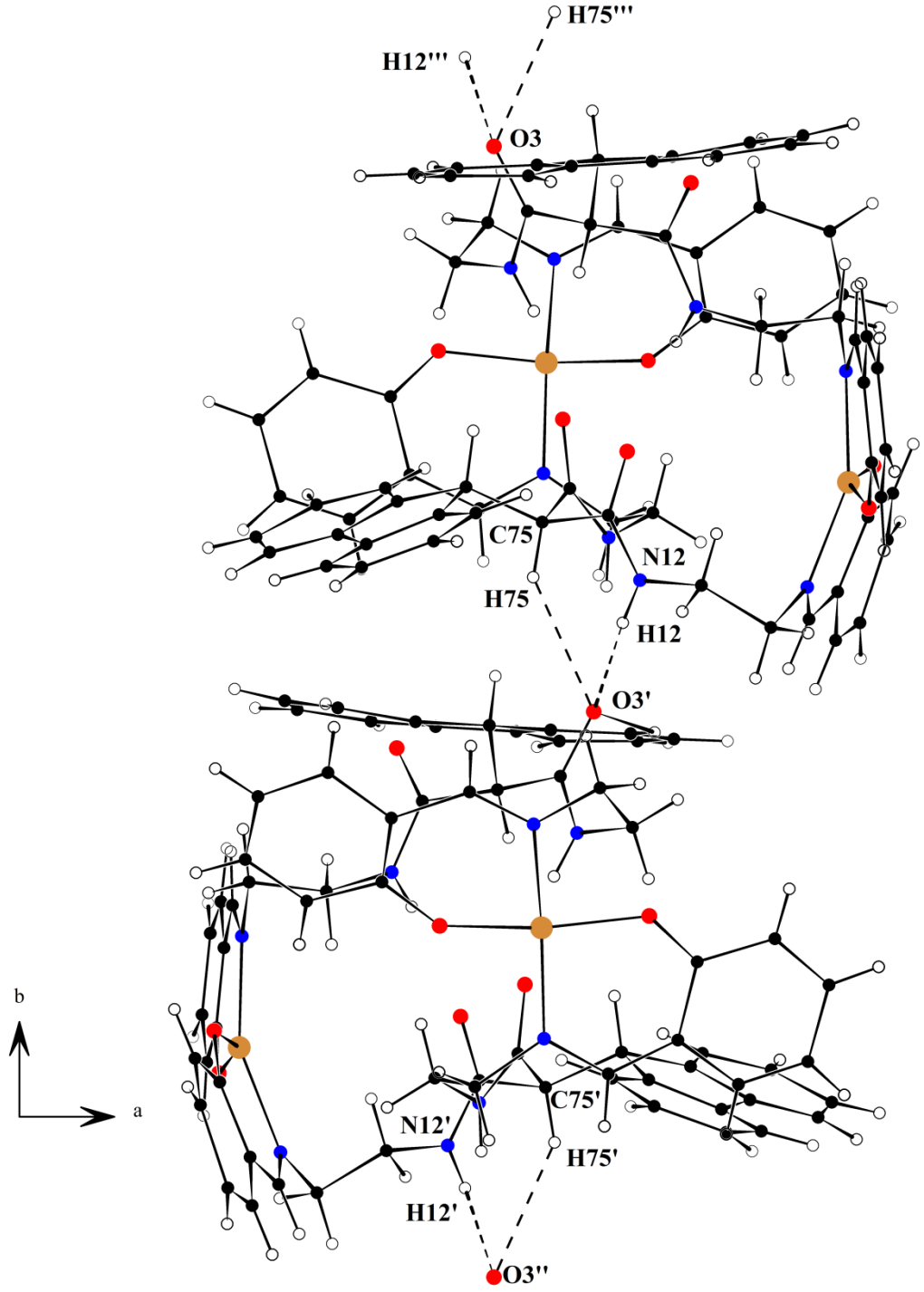

Figure 2. Section of the supramolecular arrangement of the $[Cu_2(L1)_2]$ molecules related by the along the [010] crystallographic direction in the unit cell of $[Cu_2(L1)_2]\cdot 2H_2O$ symmetry codes (′):1-*x*, -1/2+*y*, 1/2-*z* ; (″): *x*, -1+*y*, *z* ; (‴): 1-*x*, 1/2+y, 1/2-z). Radii of the represented atoms are arbitrary [40].

3.1. Characterization of compounds. Chemical composition, vibrational, ^{1}H- and ^{13}C-NMR and mass spectra.

Elemental analyses of compounds are in accordance with the assigned chemical composition of the compounds. Infrared spectra showed vibrations that are characteristic of group functions expected for these compounds, such as ν(O-H) at 3296 cm^{-1}, δ(N-H_{amide}) between 1666 and 1620 cm^{-1} and δ(C=C) at 741-727 cm^{-1} [41]. $[Mg_2(L2)](NO_3)_4$ also showed the stretching mode ν(N-O) of nitrate ions at 1332-1365 cm^{-1}. Other assignments are shown in Table 4.

Table 4. Vibrational modes of ligands L1 and L2 and their complexes.*

Assignment	L1	CuL1	MgL2	CuL2
ν(O-H), ν(N-H)	3296	3296	3331	3317
ν(C-$H_{aromatic}$)	3061, 2932	3045, 3018	3047, 2908	3035, 2902
ν(C-$H_{alifatic}$)	2863	2895	2835	2846
ν(C-H_{methyl})	-	-	2917	2910
ν(C=O_{amide}), δ(N-H_{amide}), ν(N=C)	1666, 1636	1646, 1602	1646, 1614	1635
δ(C-$O_{aromatic}$)	1261	1315	1205	1213
ν(C=$C_{aromatic}$)	1430	1529	1521	1527
π(C=$C_{aromatic}$, π(C-$H_{aromatic}$)	755-728	739-712	741-727	740-727
ν (N-$O_{nitrate}$)	-	-	1332-1365	-
ν (Cl-$O_{perchlorate}$)	-	-	-	1068
ν(Cu-N), ν(Cu-O)	-	609	-	603

*CuL1 = $[Cu_2(L1)_2]\cdot 2H_2O$; MgL2 = $[Mg_2(L2)](NO_3)_4$; CuL2 = $[Cu_2(L2](ClO_4)_4\cdot 4H_2O$

^{1}H- and ^{13}C-NMR spectra of L1 and $[Mg_2(L2)](NO_3)_4$ are seen in *Supplementary Material Section* Figures SM1-SM4, and chemical shifts and integration values in Tables SM1 and SM2. Hydrogen signals in L1 were assigned as H11 and H12 (6.844-6.888 ppm, m, 4H,), H13, H14 and H15 (7.284-7.359 ppm, m, 6H) from the phenol ring and H1 (7.833 ppm, d, 2H) and H2 (7.887, t, 2H) are from the fluorene unit. Hydrogen H7 from the amide group was not observed, due to the rapid isotopic exchange with the solvent. Signals at 3.3-3.6 ppm and at 2.5 ppm are from water and dimethylsulfoxide molecules, in that order. ^{13}C-NMR of L1 showed C14-C17 in the high frequency range of the spectrum and chemical shifts at 125.304-118.420 ppm, while C13 experience the electron withdrawing effect of both the –OH and imine (-N=C-C13) and appears at δ = 144.304 ppm. This assignment was confirmed since the signal is absent in the DEPT-135 spectrum as seen Figure SM2. Signals from carbons C5, C6 and C9 were also not seen in the DEPT-135 experiment, due to their quaternary nature.

^{1}H-NMR spectrum of $[Mg_2(L2)](NO_3)_4$ showed broad collapsed signals like H1 from the aromatic rings at 7.195-8.534 ppm (m, 28H). The integration of this region suggests a combined signal with amide and imine hydrogen atoms. The six hydrogen atoms from the methyl group resonate in high frequency at 2.156-2.350 ppm. Methylene ($-CH_2-$) and methyl ($-CH_3$) hydrogens C10, C11 and C16 resonate with δ at 39.815, 37.704 and 38.672 ppm, respectively. Phenol carbon, C17-OH, shows resonance at 168.4811 ppm, close to the value found for C18-OH at 168.069 ppm in L1. Other assignments are in Table SM2.

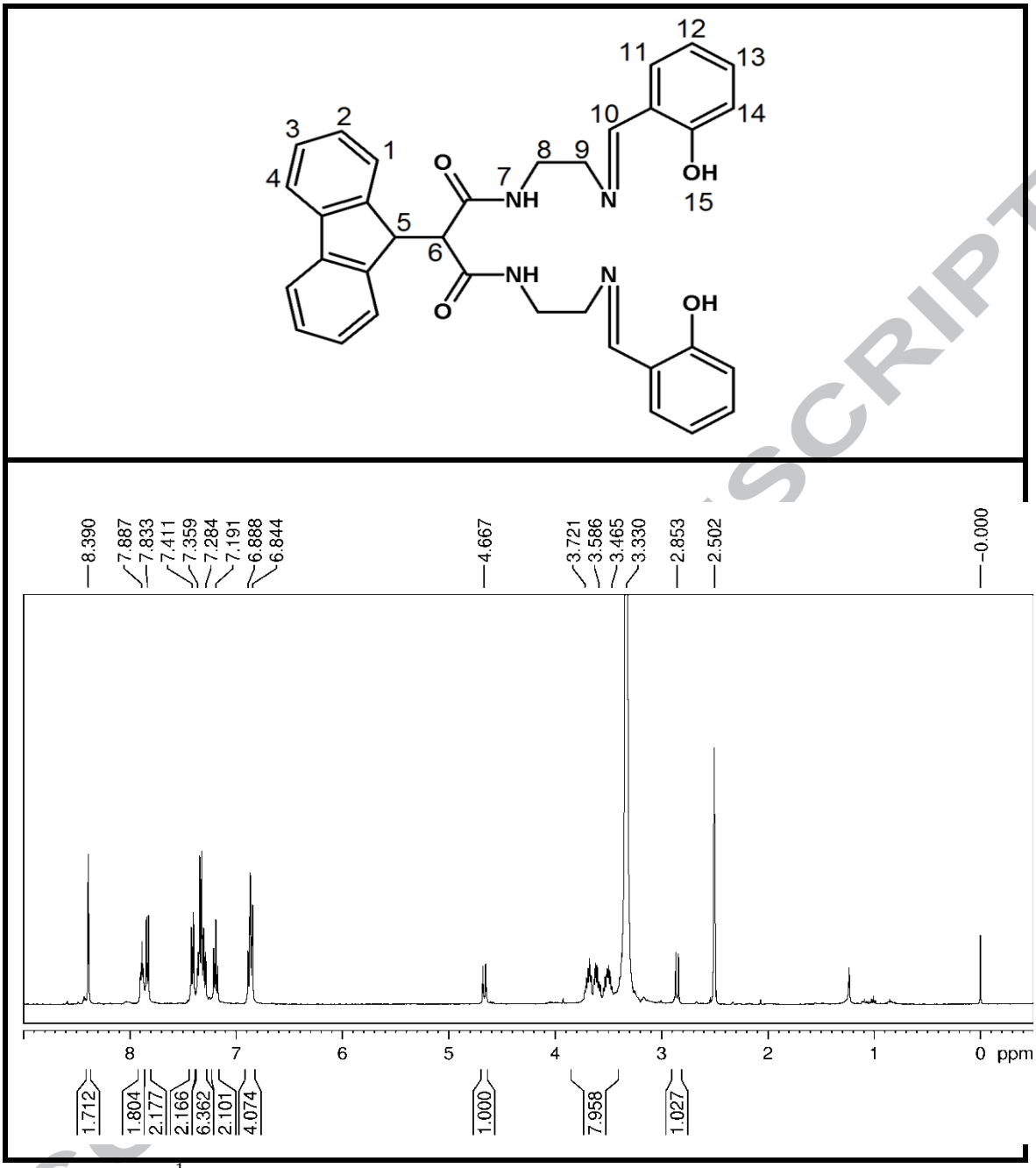

Figure SM1. ^{1}H-RMN spectrum of L1 in d_6-dmso

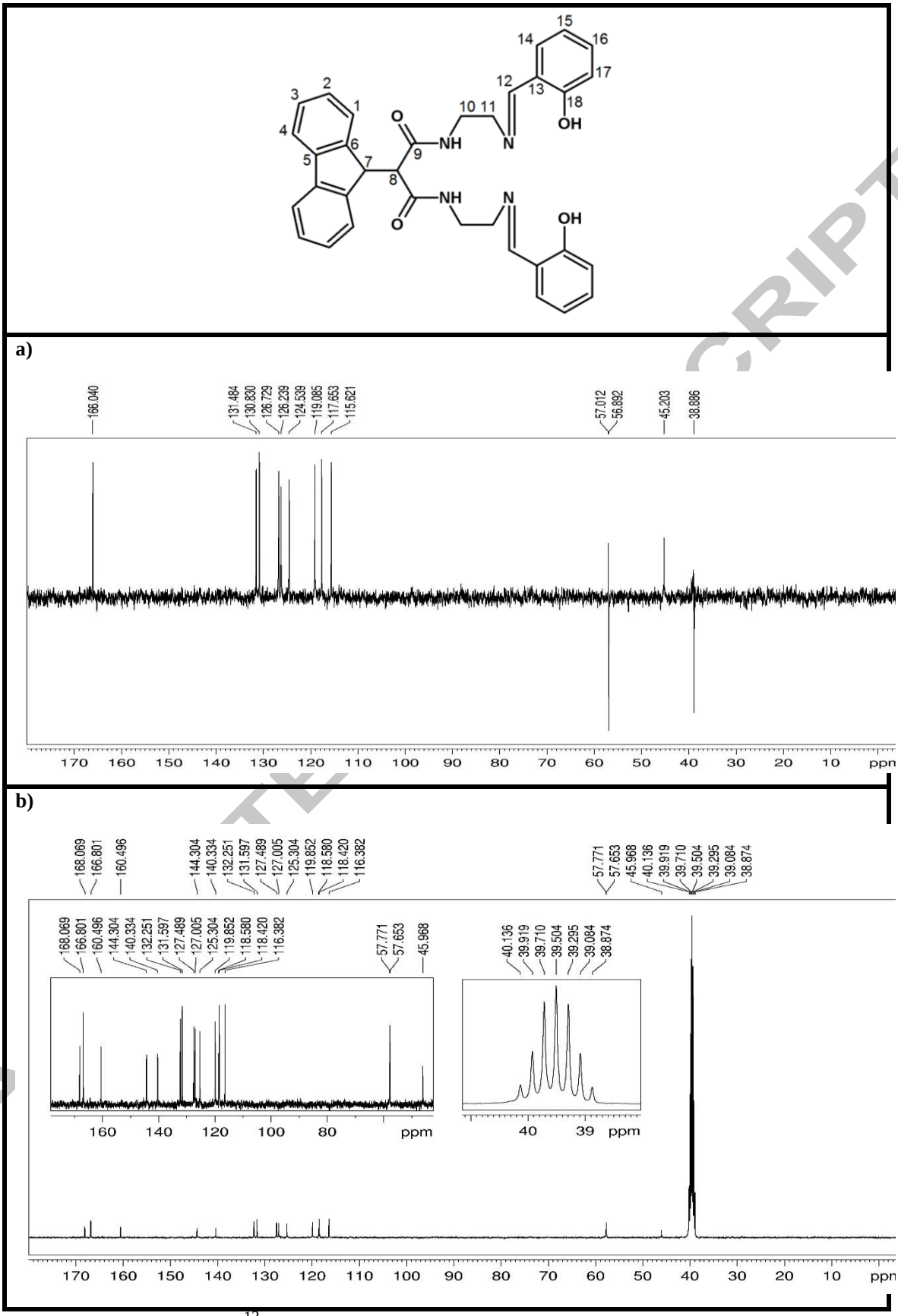

Figure SM2. a) DEPT ^{13}C-RMN spectrum of L1 in d_6-dmso; b) regular spectrum with expansion

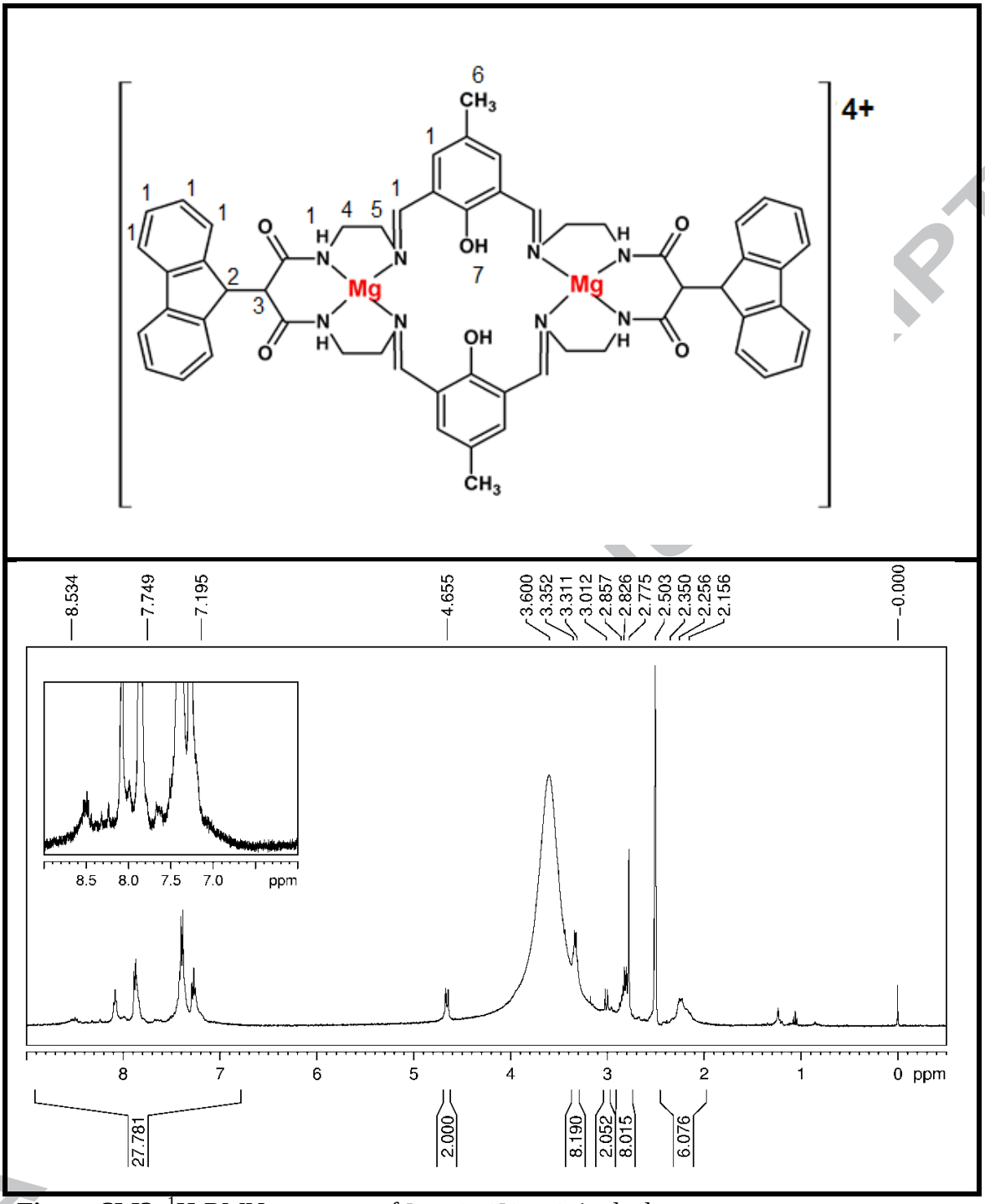

Figure SM3. ^{1}H-RMN spectrum of $[Mg_2(L2)](NO_3)_4$ in d_6-dmso.

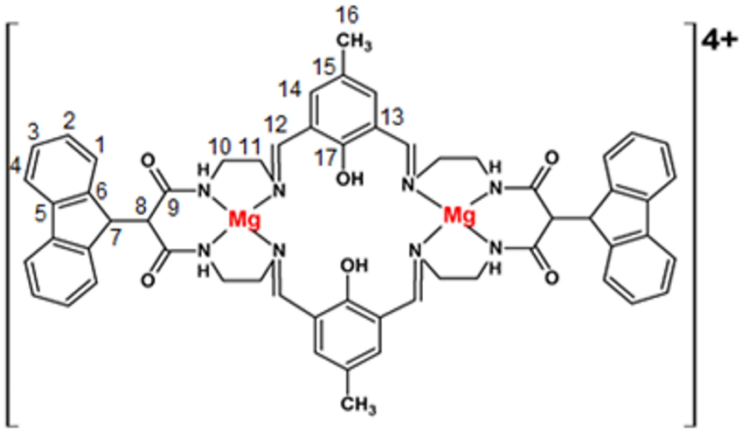

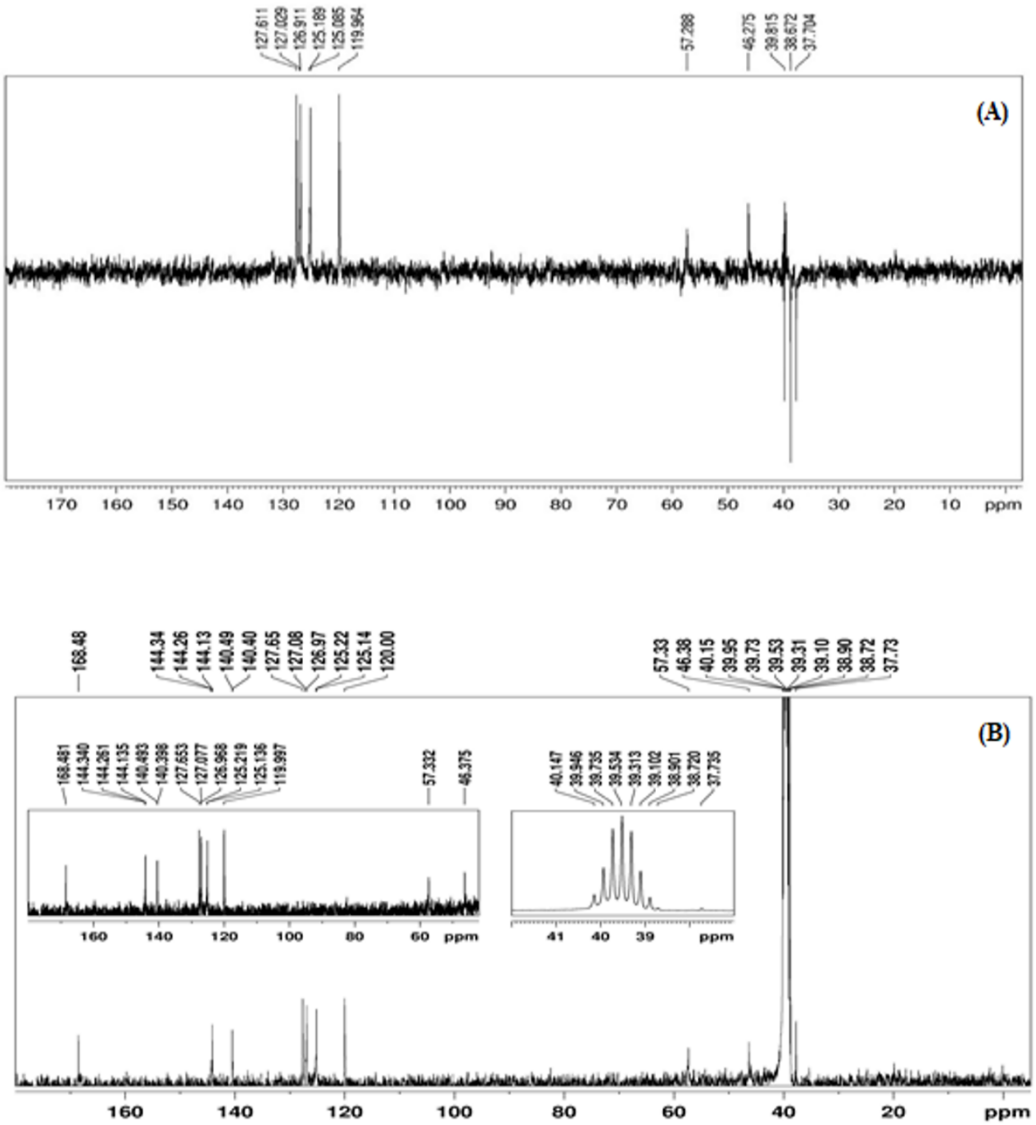

Figure SM4. a) DEPT ^{13}C-NMR spectrum of $[Mg_2(L2)](NO_3)_4$ in d_6-dmso; b) regular spectrum with expansion

Table SM1. ^{1}H- and ^{13}C-RMN data of ligand L1 in d_6-dmso.

δ(ppm)	**^{1}H[a]**	**Integration**	**δ(ppm)**	**^{13}C[b]**
2.853, d	6	1.027 (1H)	166.801	1
3.465 – 3.721, m	8, 9	7.958 (8H)	131.597	2
4.667, d	5	1.00 (1H)	127.489	3
6.844 – 6.888, m	11,12	4.074 (4H)	127.005	4
7.191, t	3	2.101 (2H)	140.334	5
7.284 – 7.359, m	13, 14, 15	6.362 (6H)	160.496	6
7.411, d	4	2.166 (2H)	57.771	7
7.833, d	1	2.177 (2H)	45.968	8
7.887, t	2	1.804 (2H)	132.251	9
8.390, s	10	1.712 (2H)	57.653	10
			masked	11
			116.382	12
			144.304	13
			125.304	14
			119.852	15
			118.580	16
			118.420	17
			168.069	18

[a] numbering refer to Figure SM1; [b] numbering refer to Figure SM2

Table SM2. ^{1}H- and ^{13}C-RMN data of $[Mg_2(L2)](NO_3)_4$ in d_6-dmso.

δ(ppm)	**^{1}H[a]**	**Integration**	**δ(ppm)**	**^{13}C[b]**
2.156 – 2.350, m	6	5.891 (6H)	127.653	1
2.775 – 2.857, m	5	8.015 (8H)	127.007	2
3.012, d	3	2.052 (2H)	126.968	3
3.311 – 3.352, m	4	8.190 (8H)	125.219	4
4.655, d	2	2.00 (2H)	144.430	5
7.195 – 8.534, m	1	27.781 (28H)	140.493	6
			57.32	7
			46.375	8
			144.135	9
			masked	10
			37.735	11
			119.997	12
			144.261	13
			125.136	14
			140.398	15
			38.720	16
			168.4811	17

[a] numbering refer to Figure SM3; [b] numbering refer to Figure SM4

High resolution mass spectrum (HRMS-ESI) of L1 in the negative mode exhibited a peak at m/z = 559.53, in accordance with the loss of H^+ and formation of $[L1\text{-}H]^-$ (Figures 3 and 5A). The spectrum of $[Mg_2(L2)](NO_3)_4$ also in the negative mode showed a peak at m/z = 209.95 assigned to a tetraaza-fragment, which is coordinated to a single magnesium ion, as seen in Figures 3 and 5B, and a low intensity peak at m/z = 982.99 due to the less stable species $[Mg(L2)\text{-}H]^-$ (Figures 3 and 5C). The spectrum in the positive mode of $[Mg_2(L2)](NO_3)_4$ showed a relatively intense signal at m/z = 961.43, attributed to $[L2]^+$ (Figures 3 and 5D). The assignments are in accordance with the calculated fragmentation patterns, considering the isotopic distribution of the elements.

The copper(II)-complexes were also characterized by ESI mass spectrometry. $[Cu_2(L1)_2(H_2O)_2]$ exhibited two sets of fragments in the negative mode at 620.15 and 1279.30, assigned to the $[Cu(L1)\text{-}H^+]^-$ and $[Cu_2(L1)_2(H_2O)_2]\text{-}H^+]^-$, respectively (Figures 4, 5E and 5F). The macrocyclic complex $[Cu_2(L2)]^{4+}$ showed a major set of signals centered at m/z = 543.14, in the positive mode, and assigned to $[Cu_2(L2)\text{-}2H^+]^{2+}$ (Figures 4 and 5G). We believe that the more symmetric tetraazacoordination is the most plausible one, as seen for the magnesium ions. However, considering the large size and high flexibility of the macrocycle ligand, an alternative mode of coordination through 3N1O could be possible and has support from the EPR measurements that will be discussed below.

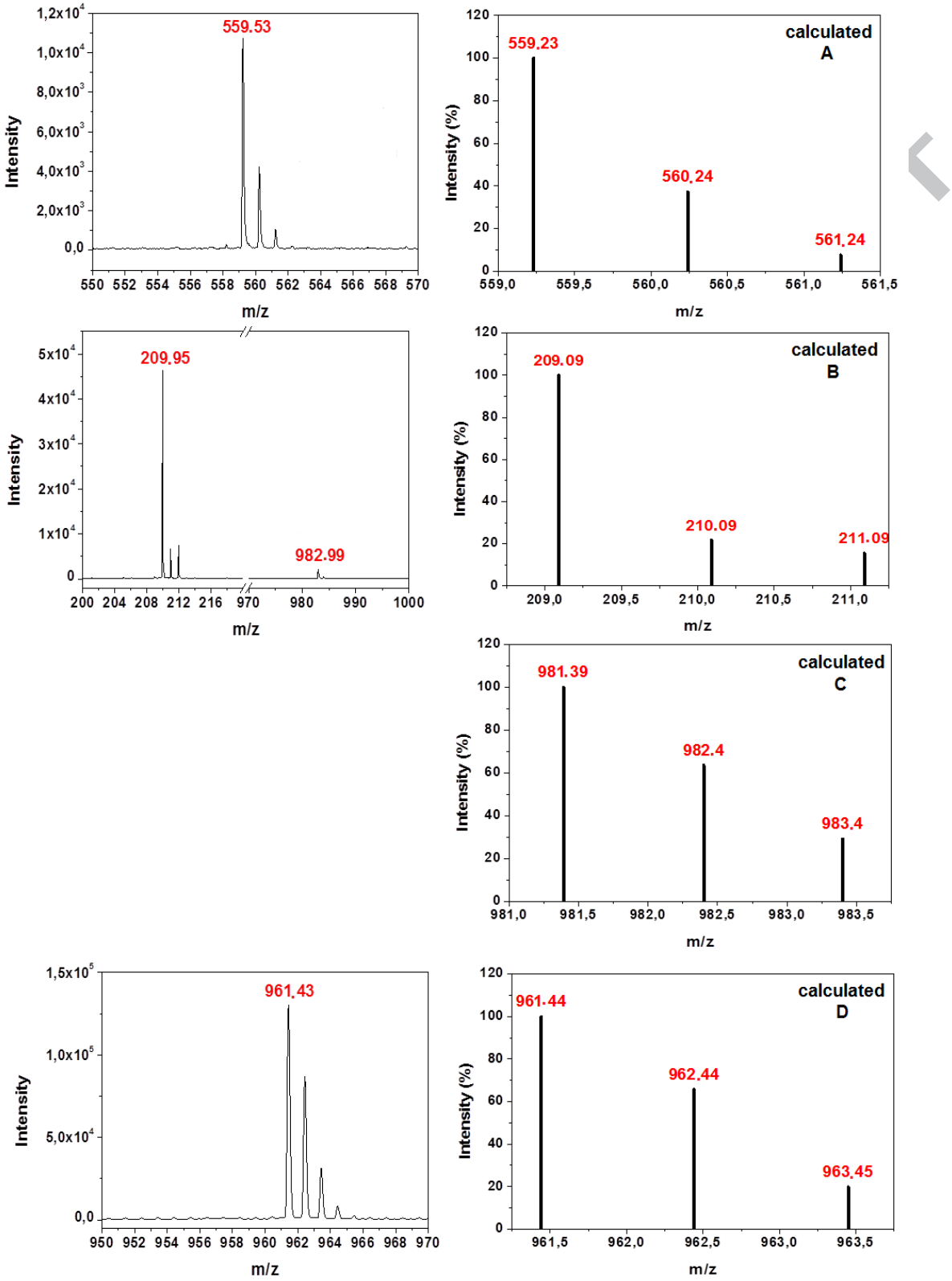

Figure 3. HRMS-ESI negative mode of (top) L1 and (middle) and (bottom) $[Mg_2(L2)](NO_3)_4$ dissolved in DMSO. Insets show the three most intense peaks of the calculated fragmentation patterns (see Figure 5) considering the isotopic distribution of the elements.

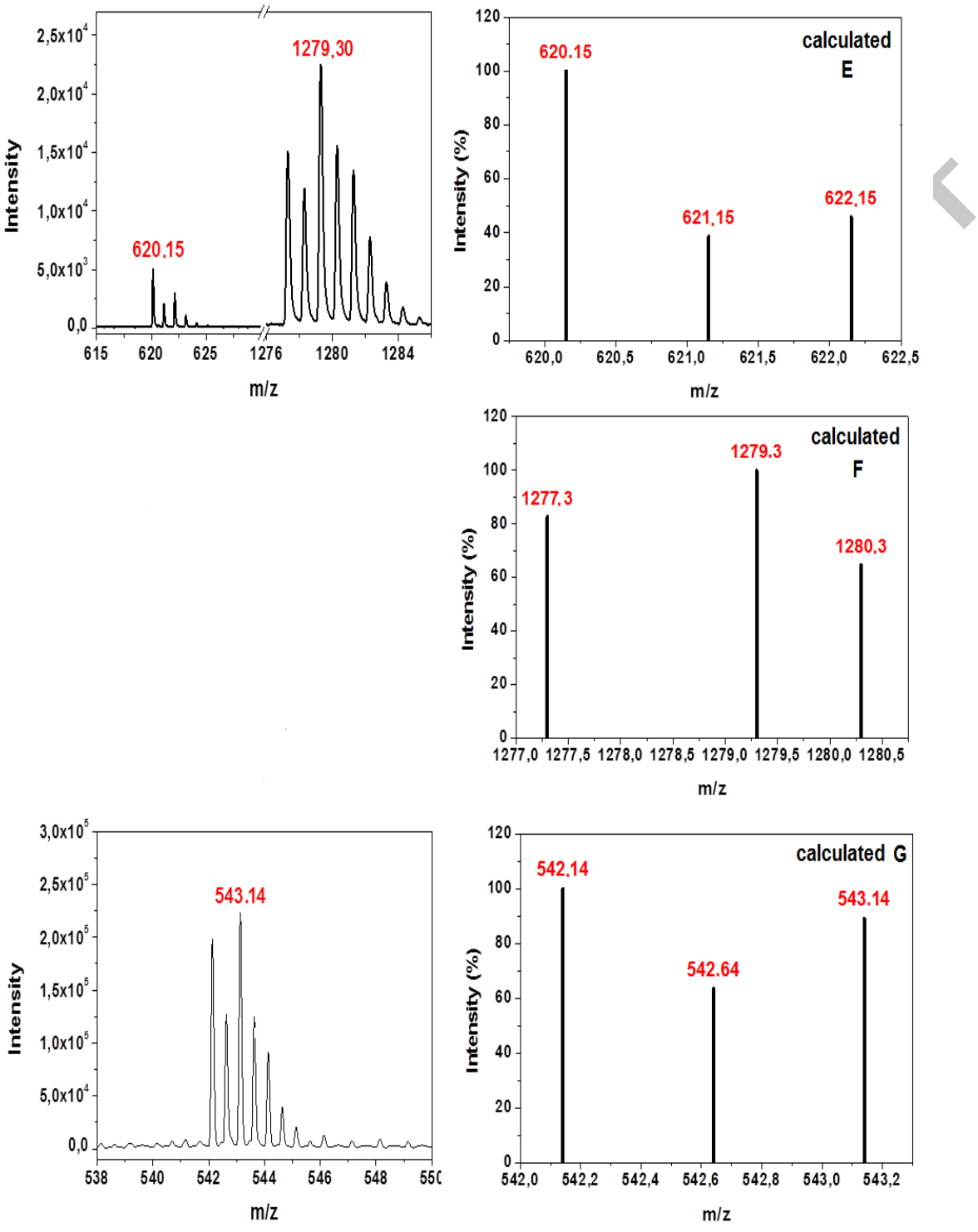

Figure 4. HRMS-ESI negative mode of (top) $[Cu_2(L1)_2]\cdot 2H_2O$ and (bottom) $[Cu_2(L2)](ClO_4)_4\cdot 4H_2O$ dissolved in DMSO. Insets show the three most intense peaks of the calculated fragmentation patterns (see Figure 5) considering the isotopic distribution of the elements.

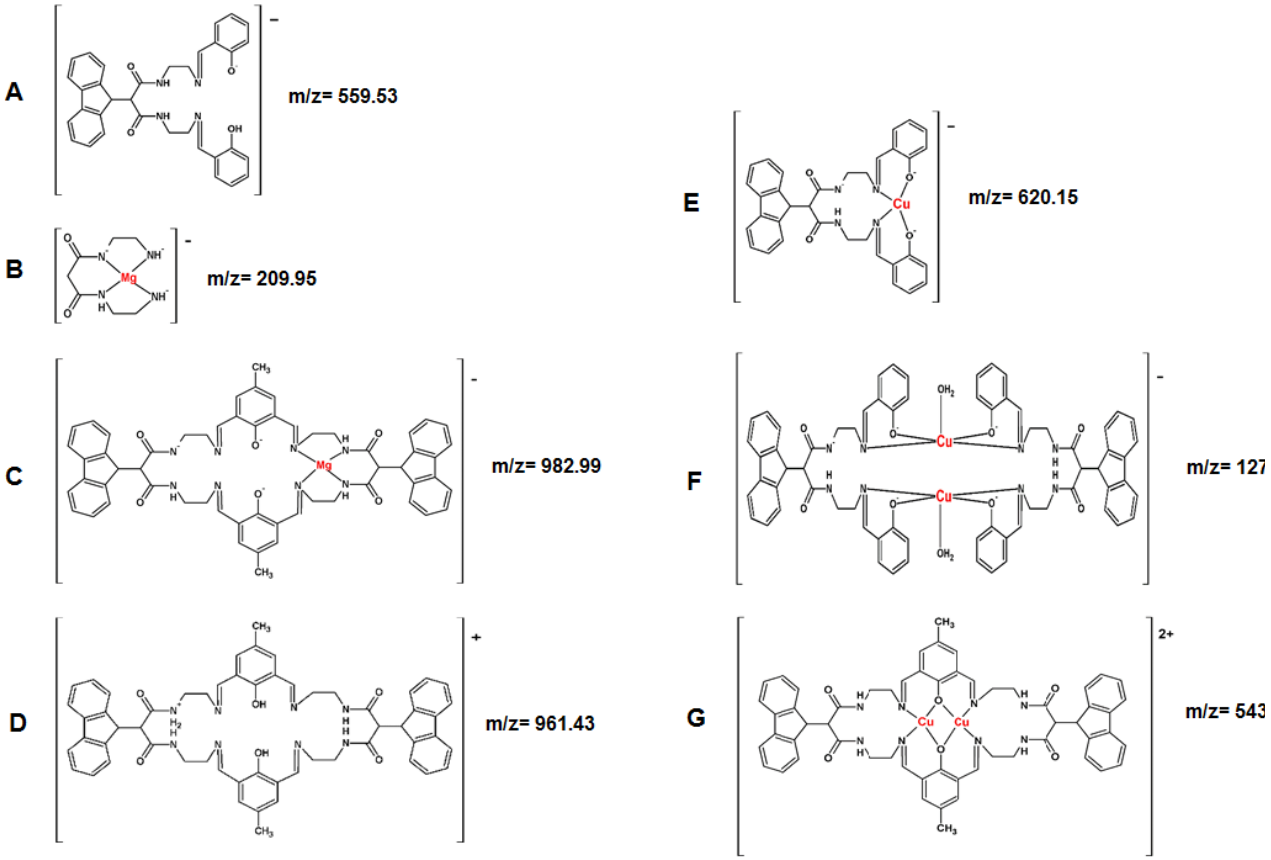

Figure 5. Molecular peaks and fragments assignments according to the experimental and calculated data in Figures 3 and 4.

EPR spectroscopy of $[Cu_2(L1)_2]\cdot 2H_2O$ and $[Cu_2(L2](ClO_4)_4\cdot 4H_2O$

Figure 6 shows the *EPR* spectra of $[Cu_2(L1)_2(H_2O)_2]$ and $[Cu_2(L2)](ClO_4)_4\cdot 4H_2O$ in the solid state and in DMSO:MeOH (1:1 v/v). The spectra of powdered samples of $[Cu_2(L1)_2(H_2O)_2]$ (Cu…Cu at 7.435 Å) does not show any half-field spin transition, which would be expected if the metal ions were magnetically coupled. The same behavior was reported in EPR investigation of other binuclear copper complexes, where the metal centers are even closer, with a Cu…Cu distance of 3.33654(11) Å [42]. In contrast, $[Cu_2(L2)](ClO_4)_4\cdot 4H_2O$ exhibits the half-field transition at a resonance field around 1700 G (Figure 6C), in accordance with the dicopper(II) composition, and suggesting the metal ions are bridged through the phenolate oxygen, as given in Figure 5G.

The *EPR* spectra from frozen solutions at 77K are characteristic of magnetically diluted mono and binuclear species and show the $m_s = -½ \rightarrow m_s = ½$ transition of a $3d^9$, S = ½ ion, which is split in four lines by the hyperfine coupling with the nuclear magnetic spin of copper ion (I = 3/2) [43]. Spectra of solutions were simulated [44] and the results are collected in Table 5. Parameters were correlated using Peisach and Blumberg [45] criteria applied to both parallel hyperfine coupling (A_z) and gyromagnetic component (g_z) to help establish the mode of coordination of the ligands. Based on this analysis, it is suggested a 2N2O and a 3N1O coordination, the oxygenated ligand coming from water, dimethylsulfoxide or a methanol molecule. It is important to emphasize that this proposal is presented for species in solution (cf. last column of table 3) and does not exclude the 4N-coordination in the solid state. The complexes showed some degree of rhombicity as given by different values of g_x, g_y and g_z, but the relation $g_z > g_{x,y}$ indicates a major axial symmetry, characteristic of the unpaired electron of copper(II) occupying the $dx^2\text{-}y^2$ orbital [45]. The rhombic character of the complexes is

most likely caused by different bond lengths between Cu(II) and the *N*- and *O*-donor atoms aggravated by the high flexibility of the ligands.

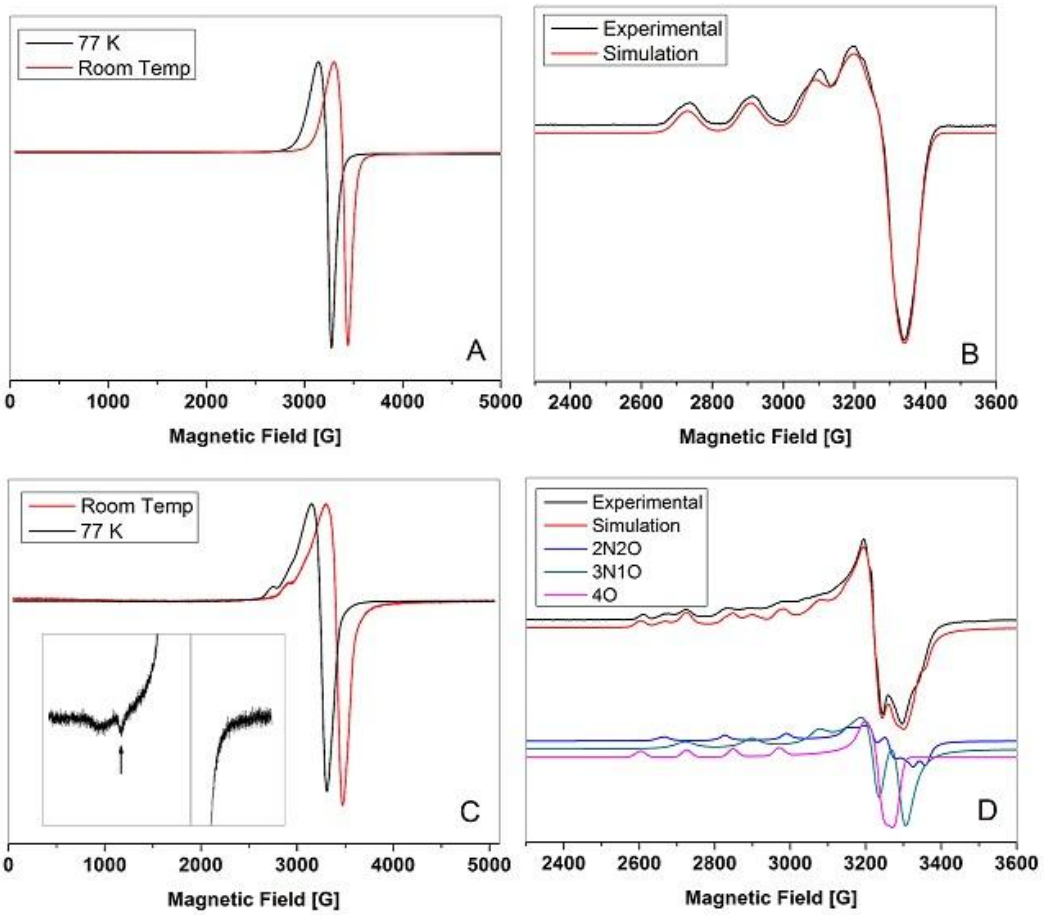

Figure 6. EPR spectra of $[Cu_2(L1)_2]\cdot 2H_2O$ (A) solid at room temperature and at 77 K; (B) in DMSO/MeOH (1:1 v/v) solution; (C) of $[Cu_2(L2)](ClO_4)_4\cdot 4H_2O$ solid at room temperature and at 77 K (inset shows the half field transition observed at 77 K); (D) in DMSO/MeOH (1:1 v/v) (the bottom spectra are the component species of the simulation, cf Table 3).

Table 5. Parameters for the EPR simulations. 77 K frozen solution spectrum simulation demonstrates a three species composition for sample Cu_2(L2), with 3N1O copper coordination scheme dominant.

		Giromagnetic tensor			*Hyperfine constant/MHz*			
	Donor atoms	g_x	g_y	g_z	A_x	A_y	A_z	**Composition fraction (%)**
$Cu_2(L1)_2$	2N2O	2.025	2.074	2.231	46.0	53.3	541	100
Cu_2(L2)	2N2O	2.015	2.083	2.300	> 20		515	21
	3N1O	2.078	2.079	2.240	> 20		544	48
	4O	2.052	2.082	2.400	> 20		404	31

Photophysics of the L1 and $[Mg_2(L2)](NO_3)_4$

The photophysical properties of L1 and $[Mg_2(L2)]^{4+}$ were measured in dimethylsulfoxide as seen in Figure 7. UV-vis spectra showed strong intraligand $\pi\rightarrow\pi^*$ and $n\rightarrow\pi^*$ transitions with maximum molar absorptivities of $4.22\text{x}10^3$ $L.mol^{-1}.cm^{-1}$ at 262 nm for ligand L1, and $2.91\text{x}10^3$ $L.mol^{-1}.cm^{-1}$ at 278 nm for $[Mg_2(L2)]^{4+}$. Excitation at 278 nm produced emission at 307 nm, which is characteristic of the fluorene chromophore.

Quantum yields (ϕ_f) of L1 and $[Mg_2(L2)]^{4+}$ were determined as 1.2% and 5.2%, respectively, by the method of Brouwer and co-workers [44] using tyrosine (ϕ_f^{ref} = 0.13 ± 0.1, 23ºC) as a reference and calculated using Equation 2.

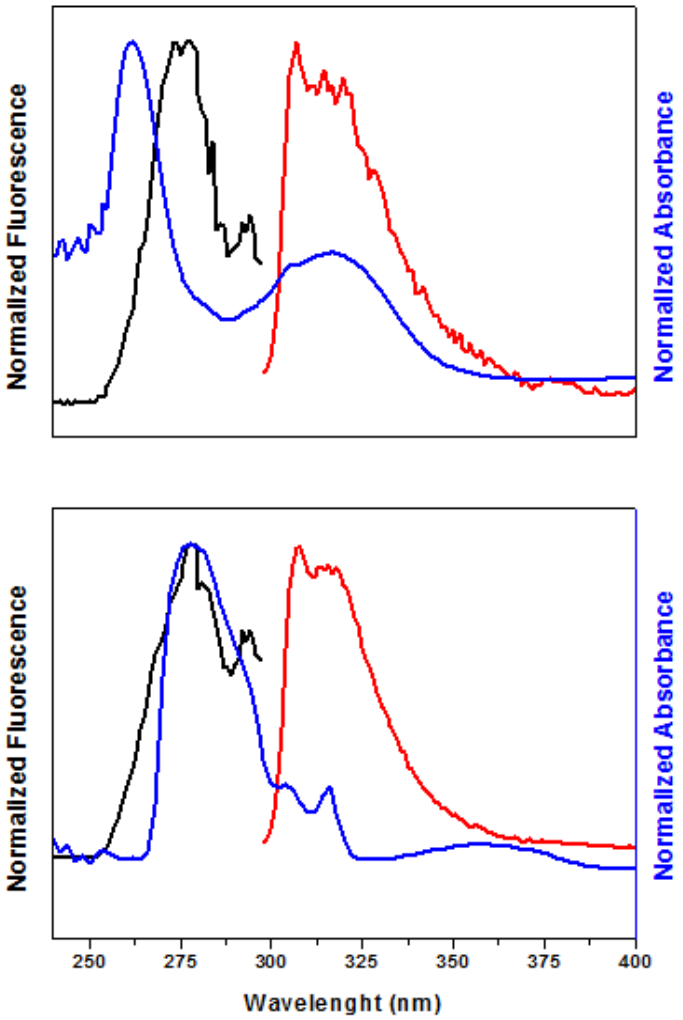

Figure 7. Normalized absorbance (blue line), excitation (black) and emission (red) spectra of L1 (top) and $[Mg_2(L2)]^{4+}$ (bottom) in 10.0 μmol.L^{-1} dimethylsulfoxide solutions,

$$\phi_f = \frac{F_s A_{ref} n_s^2}{F_{ref} A_s n_{ref}^2} \phi_f^{ref} \quad (2)$$

where *s* and *ref* refer to sample and reference, respectively; F is the area of the fluorescence spectrum; A is the absorbance at the excitation wavelength; *n* is the refractive index of the solvent (1.4793, DMSO) [47].

Coordination of L1 and L2 to copper(II) ions caused significant quenching of fluorescence as seen in Figure 8. The result is in agreement with a photoinduced electron transfer (PET) quenching mechanism [48], since d^9 copper(II) ions can participate in the electron transfer producing Cu(III), which is an accessible oxidation state. In contrast, the electron transfer mechanism is not a possibility for Mg(II) ions that have a closed shell electronic configuration, $[Ne]3s^2$.

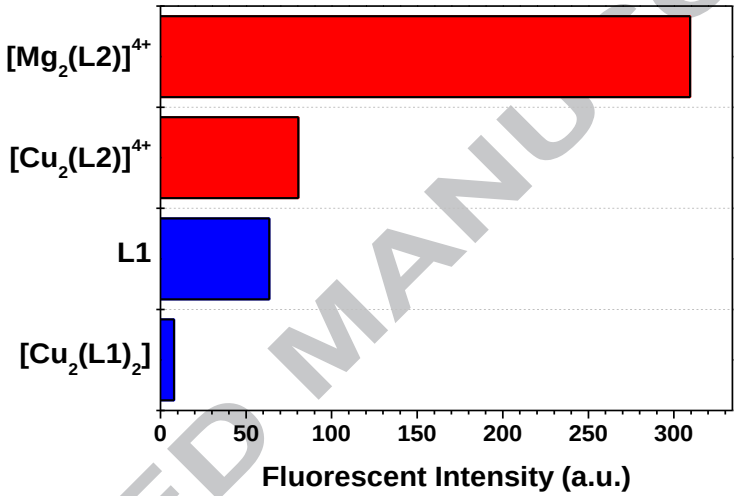

Figure 8. Fluorescence intensity of L1, $[Mg_2(L2)]^{4+}$ and the corresponding copper(II)-complexes in dimethylsulfoxide solutions.

UV-visible spectra of complexes $[Cu_2(L1)_2]\cdot 2H_2O$ and $[Cu_2(L2)](ClO_4)_4\cdot 4H_2O$ were recorded in the solid state using difuse reflectance as seen in Figure 9. Bands at 431 and 489 nm seen for $[Cu_2(L1)_2]\cdot 2H_2O$ and $[Cu_2(L2)](ClO_4)_4\cdot 4H_2O$, respectively, are due to charge transfer transitions $p\pi(\text{phenolate}) \rightarrow d\pi Cu^{2+}$ [49]. Both complexes exhibit a broad and structure-less band in the 550-920 nm range, assigned to three overlapped ligand field transitions typical of copper(II) complexes in an average octahedral field with tetragonal distortion. Gaussian line deconvolution gave a fit for transitions at 558,

674 and 788 nm for complex $[Cu_2(L1)_2]\cdot 2H_2O$ and at 624, 754 and 920 nm for $[Cu_2(L2)](ClO_4)_4\cdot 4H_2O$ due to the following transitions: (xz, yz) $\rightarrow x^2\text{-}y^2$, xy $\rightarrow x^2\text{-}y^2$ and $z^2 \rightarrow x^2\text{-}y^2$ [50].

Variation in the position of the low ligand-field energy band compared with the position of the two high-frequency bands reflects singular degrees of tetragonal distortion in the complexes. The energies of these transitions are related to the degree of the Jahn-Teller distortion and the stabilization energies (E_{JT}) were calculated as 6345 and 5435 cm^{-1} for complexes $[Cu_2(L1)_2]\cdot 2H_2O$ and $[Cu_2(L2)](ClO_4)_4\cdot 4H_2O$, respectively. Thus, the d-d bond energy can be correlated with the degree of tetragonal distortion around the copper(II) ion. The greater the distortion, the higher the energy level splitting and the Jahn-Teller stabilization energy (E_{JT}). The effect depends on the donor capacity of the axial ligand. Usually, anionic ligands produce a smaller tetragonal distortion due to a stronger metal-axial ligand bonding, along with a shorter bond distance and weak metal-equatorial bond strength. The opposite effect is expected for a stronger tetragonal distortion. See, for example, the following values of Jahn-Teller stabilization energies (in cm^{-1}: I^-(6452) < Cl^-(6477) < NCS^-(6494) < ampy(6562) < im(6614) < bipy(6685) < ampz(6739) < H_2O(7813)) observed for the series of macrocyclic complexes $[Cu^{II}(dohpn)(L)]^{n+}$, where dohpn = imineoximic tetraazamacrocyclic ligand 2,3,9,10-tetramethyl-1,4,8,11-tetraazaundecane-1,3,8,10-tetraen-11-ol-1-olate) and L = SCN^-, I^-, Cl^- (n = 0) and 4-aminopyridine (ampy), 4,4'-bipyridine (bipy), imidazole (im), 2-aminopyrazine (ampz) and water (n = 1+) [50].

The spin orbit coupling constant, λ, gives an indication of the covalence character of the metal-ligand bond. Values of λ, were estimated using published *g*-factor expressions and the energy values determined from the electronic spectra [51]. Values of λ = -428 cm^{-1} and -398 cm^{-1} for complexes $[Cu_2(L1)_2]\cdot 2H_2O$ and

$[Cu_2(L2)](ClO_4)_4 \cdot 4H_2O$, in that order, were obtained, indicating significantly smaller spin-orbit couplings than the free copper ion value at -830 cm^{-1}, and suggest a stronger covalent interaction with the copper(II) ion. Compare, for example, with -522 cm^{-1} reported for the coordination polymer $[\{Cu^{II}(HL)(H_2O)(SO_4)\}_n]$, HL = *N*,*O*-donor = pyridine-2-carbaldehyde semicarbazone ligand [52].

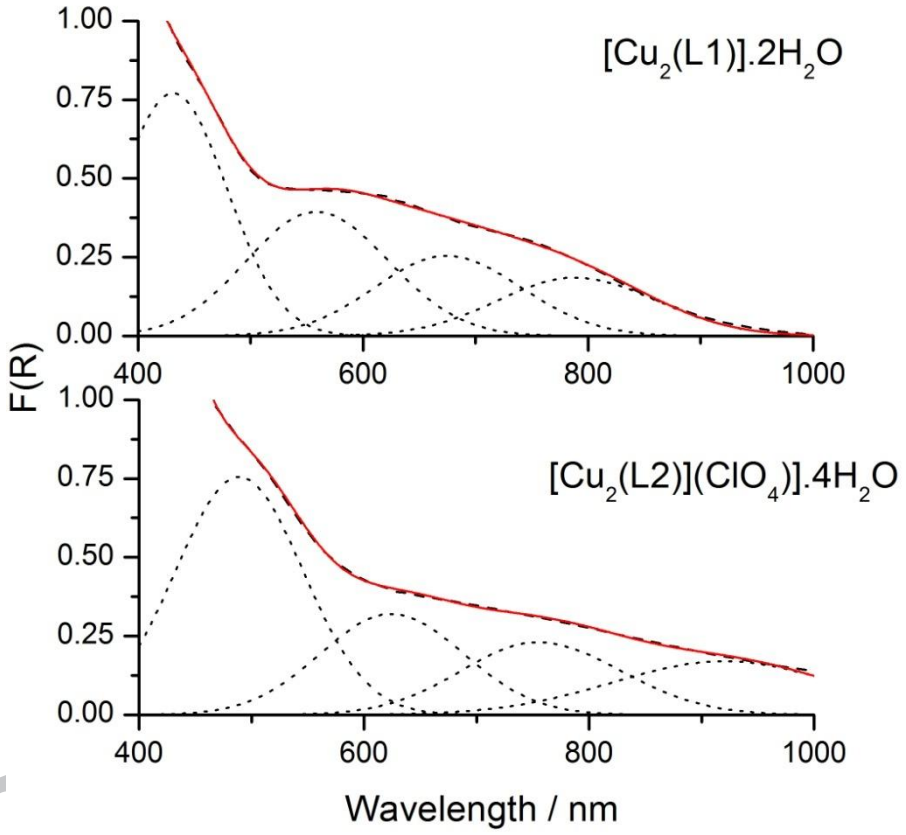

Figure 9. Difuse reflectance spectra of complexes $[Cu_2(L1)_2] \cdot 2H_2O$ and $[Cu_2(L2)](ClO_4)_4 \cdot 4H_2O$ (dashed lines). Gaussian analysis (dotted lines). The sum of Gaussian bands (red lines).

UV-visible and emission DNA-binding analysis

The interaction of fluorenyl-derivatives with ct-DNA has also been studied by absorption UV-vis spectroscopy at the 300 to 800 nm range in DMSO(1%)/PBS buffer solution. Ligand and copper(II) complexes interacts with DNA and gives a change in UV-vis spectra. The effect of different concentrations of DNA on the electronic absorption spectra of the compounds (as example compound $[Cu_2(L2)](ClO_4)_4 \cdot 4H_2O$) are presented in Figure 10.

In general, upon interaction with DNA, $[Cu_2(L2)](ClO_4)_4 \cdot 4H_2O$ copper(II) complex reveals characteristic changes (hyperchromicity) in the UV-vis absorption electronic spectra. Addition of various concentrations of ct-DNA (0 to 100 $\mu mol.L^{-1}$) caused an increase in absorbance at 364 nm and 421 nm, respectively. No red shift observed (0-2 nm) in all cases is indicative of very weak or non-observed electrostatic interaction of the Cu(II)-fluorenyl moiety and DNA. The changes of the LMCT band as seen in Figure 10 could be accounted by the interaction of the aromatic structure of the fluorescent unit of the molecule *via* hydrogen bonding with the DNA bases. This may be due to the presence of the fluorene ring in the structure that could interact with DNA bases via H-bonding, as previously reported for some cases of fluorenyl derivatives and possibly π-stacking interactions [54]. The intrinsic binding constants (K_b) of the compounds were calculated as summarized in Table 6. In the present study, fluorenyl copper(II) derivatives demonstrated a moderate binding to ct-DNA than the fluorenyl-ligand molecule following the increasing order of (K_b): L1 < $[Cu_2(L1)_2] \cdot 2H_2O$ < $[Cu_2(L2)](ClO_4)_4 \cdot 4H_2O$, respectively. Further confirmation of the binding affinity of the complexes were found in competitive-binding experiments using emission quenching method experiments to determine the displacement of the intercalating ethidium

bromide (EB) from ct-DNA. This discussion along are presented in the Supplementary Material and Figures SM5-SM8.

Table 6. Absorption and emission binding properties of the ligand and copper(II) derivatives.

Compound	*H* (%)[a]	Δλ (nm)[b]	K_b (M^{-1})[c]	K_{SV}(M^{-1})[d]
L1	65.4	2.0	2.08 x 10^3	4.88 x 10^2
$[Cu_2(L1)_2]\cdot 2H_2O$	7.3	1.0	1.13 x 10^4	9.82 x 10^2
$[Cu_2(L2)](ClO_4)_4\cdot 4H_2O$	18.4	0.0	1.36 x 10^4	5.27 x 10^2

[a]Hyperchromicity by UV-vis - *H*(%) = ($Abs_{initial}$ – Abs_{final})/$Abs_{initial}$ x 100, [b]Red Shift by UV-vis = $\lambda_{final} - \lambda_{initial}$, [c]Binding constant by UV-vis (K_b); [d]Stern-Volmer quenching constant by emission (K_{SV}).

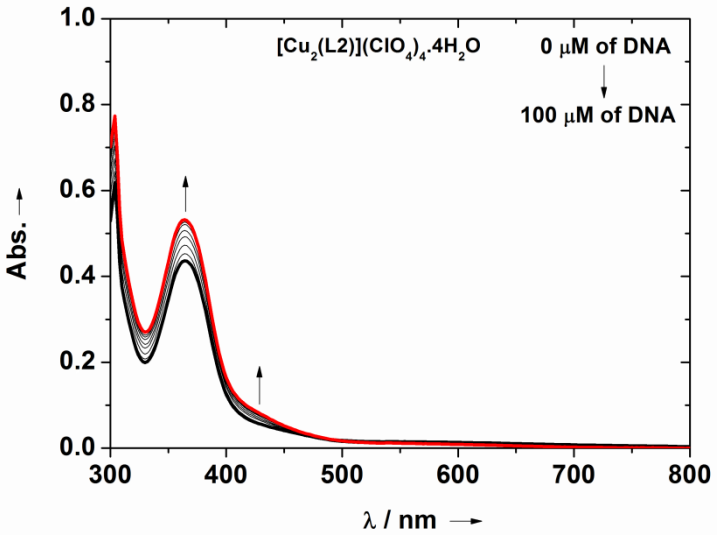

Figure 10. UV-vis titration absorption spectra of $[Cu_2(L2)](ClO_4)_4\cdot 4H_2O$ in a DMSO/PBS buffer (pH 7.4). The concentration of ct-DNA ranged from 0-100 μM.

4. Conclusions

Reaction of fluorene salicylaldehyde and 2,6-diformyl 4-methylphenol with a diamidodiamine (6-(9-fluorenyl)-1,4,8,11-tetraazaundecane-5,7-dione) produced two fluorescent sensors that were characterized by elemental analysis, ESI-MS, ^{1}H- and ^{13}C-NMR, FTIR, emission and UV-Vis spectroscopies. The compounds were used as ligands to prepared copper(II) complexes, which were also further analyzed by EPR measurements. Coordination produced a significant reduction of luminescence of the free ligands, indicating a potential use as chemosensors for copper(II) in organic media.

Single crystals of $[Cu_2(L1)_2]\cdot 2H_2O$ were isolated in orthorhombic system and space group *Pccn*. Two units of L1 bind two copper(II) ions in a tetracoordinated *N2O2* mode, through the phenolate and the imine groups. The flexible ligand wrapps around the metal center, which experiences a distorted square planar geometry. Interpretation of the electronic spectra from solid samples of $[Cu_2(L1)_2]\cdot 2H_2O$ and $[Cu_2(L2)](ClO_4)_4\cdot 4H_2O$ gave Jahn-Teller stabilization energies (E_{JT}) 6345 and 5435 cm^{-1}, respectively, and spin orbit coupling constants λ = -428 and -398 cm^{-1}. We could not obtain singles crystals suitable for X-ray diffraction analysis of complex $[Cu_2(L2)](ClO_4)_4\cdot 4H_2O$, nevertheless, its EPR spectrum exhibited a half-field $\Delta m_S = \pm 2$ transition, supporting the dicopper composition. The ct-DNA binding experiments showed that the free base fluorenyl ligand has a slightly higher affinity for the biomolecule when compared to the copper(II) derivatives.

Acknowledgements

Brazilian Research Council CNPq (Grant#401119/2016-5) supported this work. F.S.N., M.H., P.J.Z., G.A.M. and F.S.C. thank CNPq and CAPES for research fellowships. We thank UTFPR for the spectrofluorimeter.

Supplementary data

CCDC 1570863 contains the supplementary crystallographic data for this paper. These data can be obtained free of charge at www.ccdc.cam.ac.uk/conts/retrieving.html [or from the Cambridge Crystallographic Data Centre (CCDC), 12 Union Road, Cambridge CB2 1EZ, UK; fax: +44(0)1223-336033; email: deposit@ccdc.cam.ac.uk].

References

[1] H. Kozlowski, M. Luczkowski, M. Remelli, D. Valensin, Coord. Chem. Rev. 256 (2012) 2129.

[2] X. Wang, J. Tao, X. Chen, H. Yang. Sens. Actuat.B: Chem. 244 (2017) 709.

[3] S. Thavornpradit, J. Sirirak, N. Wanichacheva, J. Photochem. Photobiol. A Chem. 330 (2016) 55.

[4] N. Chatterjee, B. Mahaling, S. Sivakumar, P.K. Braradwaj, J Photochem. Photobiol. A Chem. 330 (2016) 330 110.

[5] Y.B. Wagh, A. Kuwar, S.K. Sahoo, J. Gallucci, D.S. Dalal, RSC Adv. 5 (2015) 45528.

[6] R.V. Rathod, S. Bera, M. Singh, D. Mondal, RSC Adv. 5 (2015) 34608.

[7] Y. Singh, S. Arun, B.K. Singh, P.K. Dutta, T. Ghosh, RSC Adv. 5 (2015) 80268.

[8] J. Kumar, P.K. Bhattacharyya, D.K. Das, Spectrochim. Acta A, 138 (2015) 99.

[9] M. Zhao, X-F. Yang, S. He, L. Wang. Sensors & Actuat. B.: Chem. 135 (2009) 625.

[10] H.G. Li, Z.Y. Yang, D.D. Qin, Inorg. Chem. Commun. 12 (2009) 494.

[11] Y. Xiang, Z. Li, X. Chen., A. Tong, Talanta 74 (2008) 1148.

[12] H.J. Kim, J. Hong, A. Hong, S. Ham, J.H. Lee, J.S. Kim, Org. Lett. 10, (2008) 1963.

[13] Y. Weng, Y. Teng, F. Yue, Y. Zhong, B. Ye, Inorg. Chem. Commun. 10 (2007) 443.

[14] Z. Liang, Z. Liu, L. Jiang, Y. Gao, Tetrahedron Lett. 48 (2007) 1629.

[15] J. Wu, P. Wang, X. Zhang, S. Wu, Spectrochim. Acta A 65 (2006) 749.

[16] R. Martinez, F. Zapata, A. Caballero, A. Espinosa, A. Tarraga, P. Molina, Org. Lett. 8 (2006) 3235.

[17] Y. Mei, P.A. Bentley, W. Wang, Tetrahedron Lett. 47 (2006) 2447.

[18] H-S. Kim, H-S. Choi, Talanta 55 (2001) 163.

[19] M. Beltramello, M. Gatos, F. Mancin, P. Tecillab, U. Tonellatoa, Tetrahedron Lett. 42 (2001) 9143.

[20] R. Robson, N.H. Pilkington, Aust. J. Chem., 23 (1970) 2225.

[21] M.H.Inoue, R.R. Ribeiro, J.R. Sabino, F.S. Nunes, Spectrochim. Acta, 164 (2016) 76.

[22] J.C. da Rocha, P.J. Zambiani, M. Hörner, G. Poneti, R.R. Ribeiro, F.S. Nunes, J. Mol. Struct.,1072 (2014) 69.

[23] J.C. da Rocha, G. Poneti, J.G. Ferreira, R.R. Ribeiro, F.S. Nunes, J. Braz. Chem. Soc. 25 (2014) 1528.

[24] R. B. Samulewski, J. C. da Rocha, R. Stieler, E. S. Lang, D. J. Evans, G. Poneti, K. O. R. Nascimento, R. R. Ribeiro, F. S. Nunes, Polyhedron 30 (2011) 1997.

[25] R. B. Samulewski, J.C. da Rocha, O. Fuganti, R. Stieler, E. S. Lang, M. G. F. Vaz, F. S. Nunes, J. Mol. Struct. 984 (2010) 354.

[26] L.-J. J., Q.-H. Luo, C-y. Duan, M-C. Shen, H-W. Hu, Y-J. Liu, Inorg. Chim Acta 1999 295 (1999) 48.

[27] Cao, R.H. Zhang, C. Thomas, E. Kimura, J. Chem. Soc., Dalton Trans. (1998) 2247.

[28] G.E. Jackson, P.W. Linder, A. Voye, J. Chem. Soc., Dalton Trans. (1996) 4605.

[29] X.H. Bu, Z.H. Zhang, D.L. An, Y.T. Chen, M. Shionoya, E. Kimura, Inorg. Chim. Acta 249 (1996) 125.

[30] M. Kodama, T. Koike, E. Kimura, Bull. Chem. Soc. Jpn. 68 (1995) 1627.

[31] G.D. Santis, L. Fabbrizzi, A.M.M. Lanfredi, P. Pallavicini, A. Perotti, F. Ugozzoli, M. Zema, Inorg. Chem. 34 (1995) 4529.

[32] G.D. Santis, L. Fabbrizzi, M. Licchelli, C. Mangano, D. Sacchi, Inorg. Chem. 34 (1995) 3581.

[33] L. Fabbrizzi, M. Licchelli, P. Pallavicini, A. Perotti, D. Sacchi, Angew. Chem., Int. Ed. Engl. 33 (1994) 1975.

[34] L.F. Lindoy, G.V. Meehan, N. Svenstrup, Synthesis, 7 (1998) 1029.

[35] Q.-X., Li, Y.-N., Wang, Q.-H. Luo, X.-L. Hu, Y.-Z., Li, Dalton Trans. (2008) 2487.

[36] Bruker AXS Inc., Madison, Wisconsin, USA. 2005, COSMO (Version 1.48), SAINT (Version 7.06 ^{o}), SADBS (Version 2.10).

[37] M.C. Burla, R. Caliandro, M. Camalli, B. Carrozzini, G.L. Cascarano, L. De Caro, C. Giacovazzo, G. Polidori, R. Spagna, J. Appl. Cryst. 38 (2005) 381.

[38] G.M. Sheldrick, SHELXL97: Program for Crystal Structure Solution and Refinement, University of Göttingen, Germany, 1997.

[39] M.R. Eftink, C.A. Ghiron, Anal. Biochem. 114 (1981) 199.

[40] K. Brandenburg. *DIAMOND* 3.1a. 1997 – 2005, Version 1.1a. Crystal Impact GbR, Bonn, Germany.

[41] [39] R.M. Silverstein, F.X. Webster, D.J. Kiemle, "Spectroscopic Identification of Organic Compounds", 7th ed., LTC, Rio de Janeiro, 2006.

[42] R. Gil-García, P. Gómez-Saiz, V. Díez-Gòmez, B. Donnadieu, M. Insausti, L. Lezama, J. García-Tojal, Polyhedron, 54 (2013) 243.

[43] S. Chandra, L.K. Gupta, Spectrochim. Acta., 60 (2004) 1563.

[44] S. Stoll, A. Schweiger, Journal of Magnetic Resonance, 178 (2006) 42.

[45] J. Peisach, W.E. Blumberg, Archiv. Biochem. Biophys., 165 (1974) 691.

[46] A.M. Brouwer, Pure Appl. Chem. 83 (2011) 2213.

[47] R.C., Weast, Handbook of Chemistry and Physics. 65th ed. CRC: Boca Raton, 1985

[48] L. Fabbrizzi, A. Poggi, Chem. Soc. Rev. 24 (1995) 197.

[49] R. Uma, R. Viswanathan, M. Palaniandavar, M. Lakshminarayanan, J. Chem. Soc. Dalton Trans., (1994) 1219.

[50] G. Protasiewyck, F.S. Nunes, Spectrochim. Acta A, 65 (2006) 549.

[51] A. Abragan, B. Bleaney, Electron Paramagnetic Resonance of Transition Ions, Oxford, Clarendon, 1970, pp. 458-465 and 455.

[52] E.R. Garbelini, R.R. Ribeiro, M. Hörner, A. Locatelli, F.S. Nunes, Spectrochim. Acta., 78 (2011) 1337.

[53] S. Nafisi, M. Bonsaii, V. Alexis, J. Glick, DNA Cell Biol., 30 (2011) 955.

[54] A. V. Spek, *PLATON* – A Multipurpose Crystallographic Tool, © 1980-2017, Version 290617 in *WinGX* – An Integrated System of Windows Programs for the Solution, Refinement and Analysis of Single Crystal X-Ray Diffraction Data, L. J. Farrugia, *J. Appl. Cryst.* 45 (2012), 849.

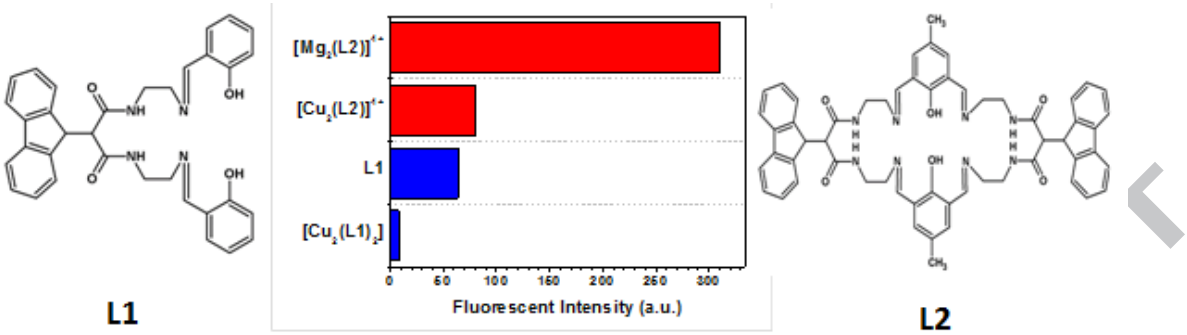

Graphical Abstract Synopsis

Synthesis and a comprehensive chemical investigation of ligands L1, L2 and their dicopper(II) complexes was performed by elemental analysis, single X-ray diffractometry, ESI-MS, ^{1}H- and ^{13}C-NMR, FTIR, EPR, UV-Vis and emission spectroscopies.